Xiaoqiang Xu

Department of Mechanical Engineering, State University of New York at Stony Brook, Stony Brook, NY 11794 e-mail: xiaoqiang.xu@stonybrook.edu

Yongjia Wu

Department of Mechanical Engineering, Virginia Tech, Blacksburg, VA 24060 e-mail: yjwu2015@vt.edu

Lei Zuo

Department of Mechanical Engineering, Virginia Tech, Blacksburg, VA 24060 e-mail: leizuo@vt.edu

Shikui Chen¹

Department of Mechanical Engineering, State University of New York at Stony Brook, Stony Brook, NY 11794 e-mail: shikui.chen@stonybrook.edu

Topology Optimization of Multimaterial Thermoelectric Structures

A large amount of energy from power plants, vehicles, oil refining, and steel or glass making process is released to the atmosphere as waste heat. The thermoelectric generator (TEG) provides a way to reutilize this portion of energy by converting temperature differences into electricity using Seebeck phenomenon. Because the figures of merit zT of the thermoelectric materials are temperature-dependent, it is not feasible to achieve high efficiency of the thermoelectric conversion using only one single thermoelectric material in a wide temperature range. To address this challenge, the authors propose a method based on topology optimization to optimize the layouts of functional graded TEGs consisting of multiple materials. The multimaterial TEG is optimized using the solid isotropic material with penalization (SIMP) method. Instead of dummy materials, both the P-type and N-type electric conductors are optimally distributed with two different practical thermoelectric materials. Specifically, Bi₂Te₃ and Zn₄Sb₃ are selected for the P-type element while Bi₂Te₃ and CoSb₃ are employed for the N-type element. Two optimization scenarios with relatively regular domains are first considered with one optimizing on both the P-type and N-type elements simultaneously, and the other one only on single P-type element. The maximum conversion efficiency could reach 9.61% and 12.34% respectively in the temperature range from 25 °C to 400 °C. CAD models are reconstructed based on the optimization results for numerical verification. A good agreement between the performance of the CAD model and optimization result is achieved, which demonstrates the effectiveness of the proposed method. [DOI: 10.1115/1.4047435]

Keywords: computer-aided engineering, conceptual design, design optimization, thermoelectric generator

1 Introduction

The thermoelectric effect refers to the direct conversion of temperature differences into the electric voltage and vice versa, which has aroused a lot of attention since its discovery. One important application of such effect is the thermoelectric generator (TEG), which can transform waste heat into electricity from various sources such as home heating, automotive exhaust, and industrial processes [1]. A TEG usually contains two semiconductors, namely P-type element (with positive charge carriers) and N-type element (with negative charge carriers). Modern TEG devices occupy unique advantages over traditional thermal power-generation devices. For instance, it can be designed in flexible size showing great scalability, operated without moving parts, and thus quite reliable and environmentally friendly [2]. Owing to these appealing features, recent years have witnessed a number of practical applications based on TEG principle, ranging from electricity generation in harsh environments such as space exploration [3], waste heat recovery in automobiles [4,5], and micro-generation for sensors or microelectronics [6,7]. However, one major weakness is that the efficiency of a TEG has been somewhat low, which, to a large extent, impedes the broader application of such technology into different fields [8].

Typically, besides the temperature difference between the hot and cold ends, the efficiency of a TEG relies heavily on the figure of merit of the thermoelectric material:

$$zT = \alpha^2 T / \rho \kappa \tag{1}$$

Contributed by the Design Automation Committee of ASME for publication in the JOURNAL OF MECHANICAL DESIGN. Manuscript received August 1, 2019; final manuscript received May 7, 2020; published online July 27, 2020. Assoc. Editor: Xu Guo.

where T is the absolute temperature, α is the Seebeck coefficient, ρ is the electrical resistivity, and κ is the thermal conductivity, respectively [9]. Several breakthroughs have been made at the nanoscale in materials science to enhance the zT. Some examples include the all-scale hierarchical architectures to reduce the thermal conductivity [10] and preparing thermoelectric materials such as Bi₂Te₃ in quantum-well super-lattice structures [11] and band engineering [12,13] to increase the power factor (α^2/ρ) . Due to these advances, the figure of merit of the TE materials could reach 1.8 with the corresponding conversion efficiency increased to 11-15% [2].

Since the thermoelectric properties are highly temperaturedependent, one thermoelectric material can only perform efficiently in a narrow temperature interval. Naturally, it is desirable to combine different thermoelectric materials together to fully exploit their respective thermoelectric capability. One typical example is the segmented thermoelectric generator [14-16], in which the P-type and N-type elements are usually divided into several segments. In each segment, a proper thermoelectric material is employed to produce the highest efficiency in the temperature interval of that segment. When designing such segmented structures, designers must ensure that the compatibility factors of different thermoelectric materials are close enough to achieve an enhanced efficiency [17]. For a segment with simple geometry, it is convenient to determine the dimensions for each segment. However, this becomes a difficult problem to treat with when it comes to a TEG with complex and irregular geometry. Besides, due to the high cost of thermoelectric materials, it is strongly desired to find the optimal distribution of a given amount of thermoelectric materials over a large domain to achieve the best performance. Topology optimization is an efficient tool for solving such materials distribution problems. Takezawa and Kitamura [18] applied the topology optimization principle to the design of

¹Corresponding author.

thermoelectric generators with a single material. Soprani et al. [19] integrated a TE cooler into a robotic tool using a 3D topology optimization and carried out the physical experiments to validate the optimized designs. Mativo and Hallinan [20] developed a compliant TEG, which can sustain mechanical loads besides performing thermoelectric functionality. Lundgaard et al. [21–24] systematically investigated the thermoelectric energy conversion problem using the SIMP method. In this paper, we aim to achieve the design of thermoelectric generators with multiple practical thermoelectric materials.

Topology optimization has emerged as a powerful conceptual design tool since its introduction by Bendsøe and Kikuchi in 1988 [25], which aims to find the optimal layout of proper materials in a prescribed design domain to obtain the best performance for a certain purpose. One remarkable characteristic of topology optimization lies in the generation of conceptual designs without depending on the designer's intuition, experience, and inspiration. Several major topology optimization approaches have been proposed over the years, including solid isotropic material penalization (SIMP) method [26,27], level set method [28,29], geometry projection method [30–33], Heaviside projection method [34] moving morphable component (MMC) method [35–37], phase field method [38], and evolutionary approach [39]. Recently, the application of topology optimization has been involved in different fields, such as the design of heat sinks [40], origami [41], or metamaterials [42]. In this paper, SIMP is employed due to its convenience in handling design variables and constraints. In the SIMP method, the design variables are usually the artificial density, based on the value of which, one can determine whether there is material or which material it is at a certain point thereby defining the topology. To implement SIMP, it is critical that the quantitative relations between the density variables and the thermoelectric properties are properly established. To be more accurate, the temperature dependence associated with the thermoelectric materials properties are taken into consideration and quantified using cubic spline interpolation functions. The output power and conversion efficiency are treated as the objectives to optimize. The sensitivity analysis is conducted using the adjoint technique, and the design is updated based on the method of moving asymptotes (MMA) algorithm [43]. In this study, two scenarios with relatively regular domains are first investigated. The first case focuses on optimizing both the P-type and N-type elements at the same time. In the other case, only the P-type element is optimized. The performance of the achieved designs are verified by implementing 2.5D FEA on recreated CAD models. Then, the proposed methodology is extended to a more practical and irregular fan-shaped TEG design. The optimized fan-shaped TEG units are conformally mapped to a hot pipe surface attempting to recover the waste heat. The performance of this conformal TEG device is also simulated and discussed.

This paper is organized as follows: in Sec. 2, the governing equations for thermoelectric phenomena are introduced. The topology optimization formulation is given in Sec. 3, including computational model description, objective functions, and material interpolation scheme. Section 4 details the numerical implementation, followed by the topology optimization results and 2.5D numerical verification in Sec. 5. A conformal TEG example intended for waste heat recovery for hot pipes is provided in Sec. 6. Finally, in Sec. 7, some concluding remarks are given.

2 Thermoelectric Governing Equations

A typical TEG, shown in Fig. 1, usually consists of heat source, heat sink, P-type and N-type thermoelectric elements, external load, and electrodes (given by gray bars with arrows in the figure). It works based on the Seebeck effect, where an electromotive force is generated due to the movement of charge carriers in the presence of a temperature gradient between the hot and cold ends. When connected to an external load to build a circuit, there will be a current flowing through to produce electric power. For P-type, the current is carried

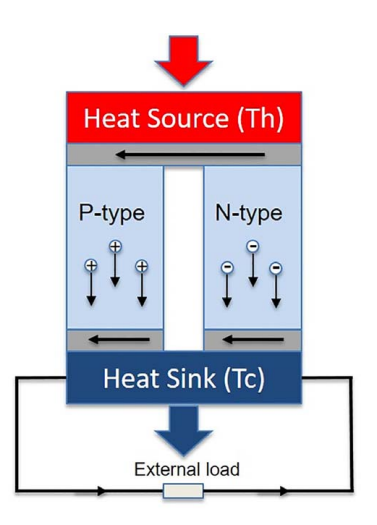


Fig. 1 The configuration of a typical TEG device

by holes, while for N-type, it is by electrons. Potentially, such a TEG device can be applied wherever there is a temperature gradient.

This multi-physics optimization problem involves heat transfer in solids, electron migration, and thermoelectric effect. For simplicity, we only consider the steady-state and assume that the thermoelectric materials are isotropic with regards to the thermoelectric properties like Seebeck coefficient, electrical conductivity, and thermal conductivity. Consulting Refs. [18,44], the governing equations for electrical and thermal conductions can be given as follows:

$$\nabla \cdot \boldsymbol{J} = 0 \tag{2}$$

$$\nabla \cdot \mathbf{q} = f \tag{3}$$

Equations (2) and (3) are coupled with the following thermoelectric constitutive equations:

$$\boldsymbol{J} = \sigma(\boldsymbol{E} - \alpha \nabla T) \tag{4}$$

$$q = \beta J - \kappa \nabla T \tag{5}$$

where J is the electric current density vector, A/m^2 ; q is the heat flux density vector, W/m^2 ; $f = J \cdot E$ is the heat generation rate per unit volume, W/m^3 ; σ is the electric conductivity, S/m; $E = -\nabla V$, electric field intensity vector, V/m; V is the electric potential, V; α is the Seebeck coefficient, V/K; T is the absolute temperature field, K; and $\beta = T \cdot \alpha$ denotes the Peltier coefficient, V; and κ is the thermal conductivity, $W/(m \cdot K)$.

The boundary conditions are as follows:

$$V = V_0$$
, fixed electric potential (6a)

$$T = T_c$$
, fixed temperature (6b)

$$T = T_h$$
, fixed temperature (6c)

$$\mathbf{n} \cdot \mathbf{J} = 0$$
, electrical insulation (6d)

$$\mathbf{n} \cdot \mathbf{q} = 0$$
, thermal insulation (6e)

By imposing the above boundary conditions, Eqs. (2) and (3) can be solved with respect to the two state variables T and V, which will be further used to compute the objective functions and constraints.

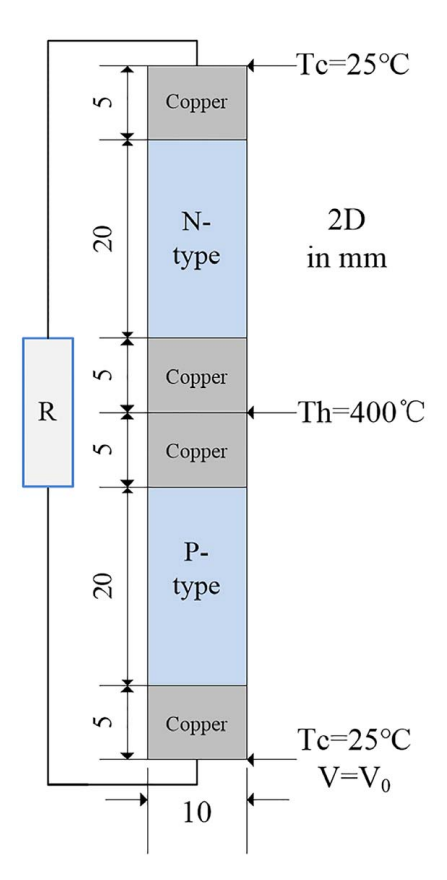


Fig. 2 Diagram of the computational model

3 Topology Optimization Formulation

Topology optimization has been a robust tool for finding the optimal materials layout for a particular purpose. In this paper, different thermoelectric materials are to be optimally distributed in the P-type and N-type thermoelectric elements, i.e., the design domain. For simplicity, only 2D problem is considered in the topology optimization stage.

3.1 Computational Model Description. As seen in Fig. 2, a 2D computational model is built. Unlike the conventional configuration in Fig. 1, this model adopts a stack junction, which could reduce the parasitic losses from the connection between the P-type and N-type electrical conductors [8]. The thickness is 1 mm to make it a thin plate structure. The temperature for the hot and cold end is set to be 400 °C and 25 °C, respectively. An electrical potential V_0 is assigned to the bottom surface. Copper acts as electrodes. An external load R is connected to form an electrical circuit and produce power. All other outer boundaries of the whole domain are electrically insulated and adiabatic, corresponding to the Neumann boundary conditions in Eqs. (6d) and (6e).

3.2 Design Objective. In this topology optimization problem, we have two objective functions to optimize, namely, output power or conversion efficiency. When there are a large amount of heat sources, maximum output power is preferably wanted. When the heat source is limited, we prefer a maximum conversion efficiency, which is defined as the ratio between output power and the total heat flow from the source. For output power:

$$P_{out} = \int_{\Omega_1} \mathbf{J} \cdot \mathbf{E} d\Omega \tag{7}$$

where J is the electric current density vector, E is the electrical field intensity vector as mentioned in Sec. 2, and Ω_1 is the external resistor domain.

The conversion efficiency is defined as follows:

$$\eta = \frac{P_{out}}{Q} = \frac{\int_{\Omega_1} \mathbf{J} \cdot \mathbf{E} d\Omega}{|\int_{\Omega_2} \mathbf{q} \cdot \mathbf{n}_1 d\Omega|}$$
(8)

where Q is the total heat flow from the source, q is the heat flux density vector, Ω_2 is the domain from which the heat flows in; and n_1 is the normal vector of Ω_2 .

Thus, the objective of the topology optimization problem is to maximize either the output power or the conversion efficiency, which can be formulated as follows:

maximize
$$J_1 = P_{out}$$
 (9)

or maximize
$$J_2 = \eta$$
 (10)

subject to:

$$\int_{\Omega_{PN}} dx \le V_f \cdot A \tag{11}$$

In the above equations, Ω_{PN} refers to regions occupied by thermoelectric materials of the final design; V_f is the volume fraction, which is set to be 0.8; and A is the initial area of the P-type and N-type elements. In practice, a large number of TEG units would be connected electrically in series and thermally in parallel to produce massive power, requiring more thermoelectric materials [6]. One potential application of this study is to harvest the waste heat from exhaust pipes of vehicles. It is then desired to reduce the mass for a single TEG unit to keep lightweight in the assembled TEG system. Therefore, it is advisable to impose a volume constraint in the designing process of a TEG unit taking the total cost and weight into consideration.

3.3 Material Interpolation Scheme. The crux of the SIMP method is that a proper relationship between the design variables and corresponding physical properties must be established. In this paper, both the P-type and N-type thermoelectric elements are to be optimized. Since there could be three different phases, namely, relatively high-temperature material, relatively low-temperature material and void, two design variables are required to distinguish them. Following Refs. [45,46], we employ the following material interpolation scheme in this paper:

$$\alpha(\rho_{1}, \rho_{2}) = \rho_{1}^{p}(\rho_{2}^{p}\alpha_{1} + (1 - \rho_{2}^{p})\alpha_{2})$$

$$\kappa(\rho_{1}, \rho_{2}) = \rho_{1}^{p}(\rho_{2}^{p}\kappa_{1} + (1 - \rho_{2}^{p})\kappa_{2})$$

$$\sigma(\rho_{1}, \rho_{2}) = \rho_{1}^{p}(\rho_{2}^{p}\sigma_{1} + (1 - \rho_{2}^{p})\sigma_{2})$$
(12)

where $0 < \rho_{\min} \le \rho_1 \le 1$, $0 < \rho_{\min} \le \rho_2 \le 1$; ρ_{\min} is a small positive parameter to avoid singularity; and p is the penalty factor and is set to be 3. The symbols α_i , κ_i , σ_i , i=1,2 denote the Seebeck coefficient, thermal conductivity, and electrical conductivity of the two thermoelectric materials, respectively. At each point of the design domain, there are two design variables, where ρ_1 is used to determine whether it is material or void and ρ_2 is used to indicate which material it is. The penalty factor p is employed to enforce the densities toward ρ_{\min} or 1. Nevertheless, only in ideal cases will the final densities be either ρ_{\min} or 1. In practice, a transition region with intermediate densities between material and void domain would always exist. In this paper, a threshold is set to manually separate three phases. This will be discussed in detail in Sec. 5.

4 Numerical Implementation

The procedures of the topology optimization process are shown in Fig. 3. To perform the numerical implementation, the governing equations must be solved correctly to obtain the state fields, i.e., temperature and electrical potential fields in this case and further to compute the objective functions and constraints. If it is not converged, sensitivity analysis needs to be conducted and later to

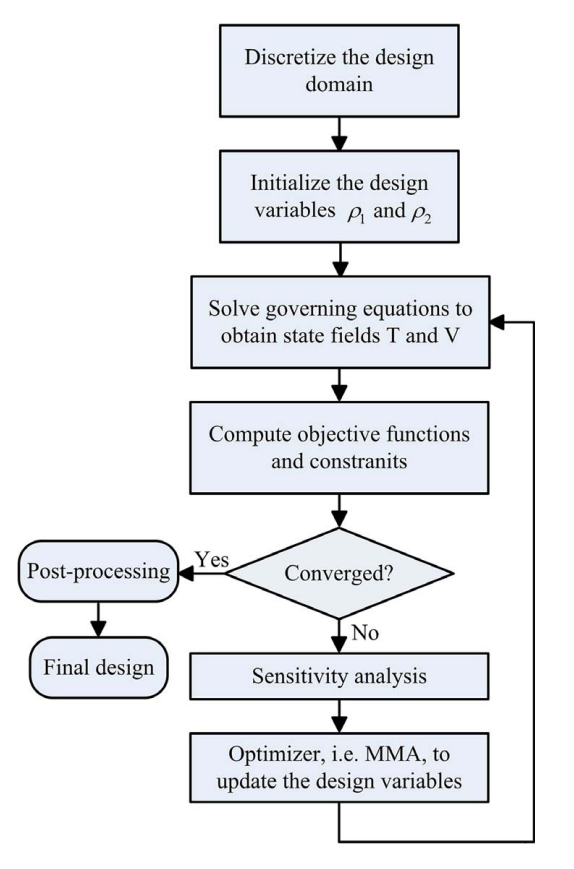


Fig. 3 The flowchart for the topology optimization process

Table 1 Material selection

P-type	Bi ₂ Te ₃	Zn ₄ Sb ₃
N-type	Bi ₂ Te ₃	CoSb ₃

update the design variables using the method of moving asymptotes (MMA) algorithm [43]. After convergence, post-processing steps, like smoothing the boundary to facilitate the manufacturing process, need to be included before the final design is presented. The above procedures are realized with the COMSOL MULTIPHYSICS FEA software.

4.1 Thermoelectric Material Properties. The thermal and electronic properties of the copper electrodes are as follows: $\alpha = 6.5 \times 10^{-6}$ V/K, $\kappa = 400$ W/(m·K), and $\sigma = 5.998 \times 10^{7}$ S/m. Because the temperature ranges from $T_c = 25$ °C to $T_h = 400$ °C, two different thermoelectric materials are employed for each of the P-type and N-type elements, as shown in Table 1 based on the zT value from Ref. [47]. Such selection makes sure that there are a low-temperature and high-temperature thermoelectric material relatively for each type element, making it possible to make the most of the thermoelectric capability of each material.

The temperature dependency of thermoelectric materials properties is taken into account and plotted based on the data from Ref. [47] in Fig. 4. For a certain thermoelectric material, the thermoelectric properties data are available in the narrow temperature range where the figure of merit zT is high. Beyond that temperature range, the thermoelectric properties are extrapolated using the nearest function. As seen from Fig. 4(d), a certain TE material has a high zT in its working temperature interval and a much smaller zT value by extrapolation (not shown) in other temperature range. And the efficiency of a TEG relies strongly on the zT values. Intuitively, we can imagine a design where the relatively high-temperature materials, i.e., Zn_4Sb_3 and $CoSb_3$ are distributed near the hot end while the relatively low-temperature materials, i.e., Bi_2Te_3 near the cold end. In practical implementation, the thermoelectric properties are interpolated using cubic spline functions.

4.2 Finite Element Formulation. The governing equations are highly nonlinear due to the coupling of electrical and thermal conductions as well as the strong temperature dependence of the thermoelectric materials properties. They are solved in discretized

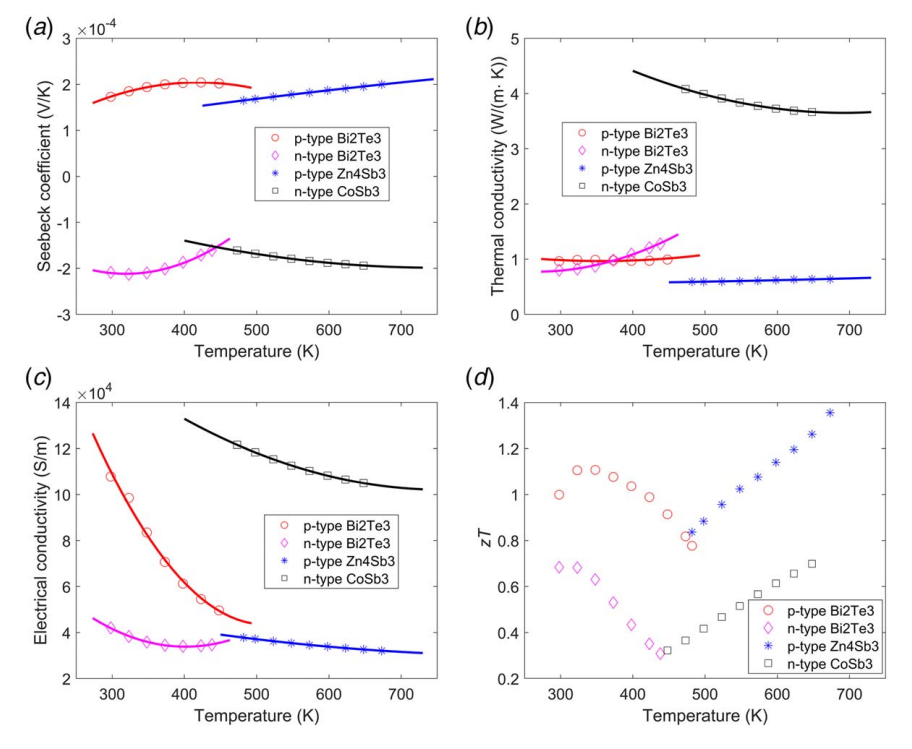


Fig. 4 Thermal and electronic properties of thermoelectric materials: (a) Seebeck coefficient, (b) thermal conductivity, (c) electrical conductivity, and (d) figure of merit

forms by standard finite element method [48].

$$\begin{bmatrix} \mathbf{K}^{VT} & \mathbf{K}^{VV} \\ \mathbf{K}^{TT} & \mathbf{0} \end{bmatrix} \begin{Bmatrix} \mathbf{T}^{n} \\ \mathbf{V}^{n} \end{Bmatrix} = \begin{Bmatrix} \mathbf{0} \\ \mathbf{Q}^{P} + \mathbf{Q}^{E} \end{Bmatrix}$$
 (13)

$$\mathbf{K}^{VT} = \sum_{1}^{n} \int_{\Omega^{e}} [\mathbf{B}]^{T} \alpha \sigma[\mathbf{B}] d\Omega^{e}$$
 (14a)

$$\mathbf{K}^{VV} = \sum_{1}^{n} \int_{\Omega^{e}} [\mathbf{B}]^{T} \sigma[\mathbf{B}] d\Omega^{e}$$
 (14b)

$$\mathbf{K}^{TT} = \sum_{1}^{n} \int_{\Omega^{e}} [\mathbf{B}]^{T} \lambda [\mathbf{B}] d\Omega^{e}$$
 (14c)

$$\mathbf{Q}^{P} = \sum_{1}^{n} \int_{\Omega^{e}} [\mathbf{B}]^{T} \beta [\mathbf{J}] d\Omega^{e}$$
 (14*d*)

$$\mathbf{Q}^{E} = \sum_{1}^{n} \int_{\Omega^{e}} [\mathbf{N}]^{T} [\mathbf{J}]^{T} [\mathbf{E}]^{T} d\Omega^{e}$$
 (14e)

where \mathbf{T}^n , \mathbf{V}^n represent the nodal temperature and nodal electrical potential vector, respectively. N is the linear shape function and $\mathbf{B} = \nabla N$. The finite element analysis is performed using mapped quadrilateral elements with a maximum element size 0.4 mm. The total domain element number is 3850.

The above discretized system is obtained following the general procedures: first multiply the original governing equations with test functions, integrate over the whole domain by parts, and utilize the 2D divergence theorem.

4.3 Sensitivity Analysis. The sensitivity information, i.e., the total derivative of objective functions with respect to the design variables, must be derived to update the design in each iteration. In this paper, the adjoint method [49] is employed, which starts from the discretized system as shown in Sec. 4.2. Equation (13) can be rewritten in the following residual form:

$$\mathbf{R}(\rho, \mathbf{U}) = \mathbf{K}(\rho, \mathbf{U}) \cdot \mathbf{U} - \mathbf{F}(\rho, \mathbf{U}) \tag{15}$$

where R is the residual vector, K is the global stiffness matrix, U is the state variable vector, i.e., $\{T, V\}$ in this case, and F is the global load vector.

Then, the general Lagrangian function can be formulated as follows:

$$\mathbf{L}(\rho, \mathbf{U}) = J(\rho, \mathbf{U}) + \lambda^T \cdot \mathbf{R}(\rho, \mathbf{U}) \tag{16}$$

 λ^T is the Lagrangian multiplier. The differentiation of the objective function J in relation to design variable ρ is calculated by

$$\frac{dJ}{d\rho} = \frac{d\mathbf{L}}{d\rho} = \frac{\partial J}{\partial \rho} + \frac{\partial J}{\partial \mathbf{U}} \cdot \frac{d\mathbf{U}}{d\rho} + \lambda^T \cdot \left[\frac{\partial \mathbf{R}}{\partial \rho} + \frac{\partial \mathbf{R}}{\partial \mathbf{U}} \cdot \frac{d\mathbf{U}}{d\rho} \right]$$
(17)

The crucial point of the adjoint method in conducting sensitivity analysis is to get rid of the derivative of the state variables with respect to the design variables, which can be done by solving the following adjoint equation for proper λ^T :

$$\lambda^T \cdot \frac{\partial \mathbf{R}}{\partial \mathbf{U}} = -\frac{\partial J}{\partial \mathbf{U}} \tag{18}$$

Once λ^T is obtained, we can get the sensitivity information from equation (17).

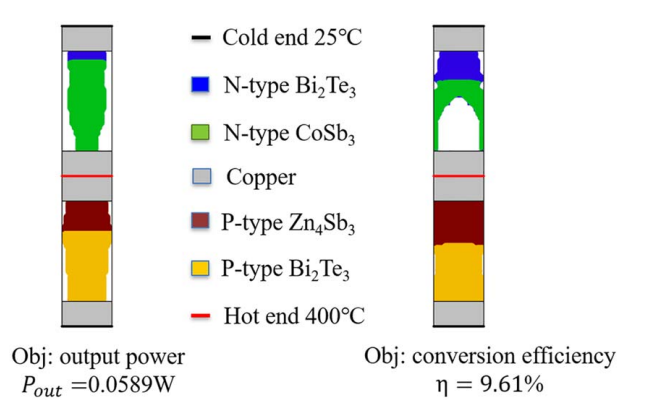


Fig. 5 Topology optimization with P-type and N-type materials

5 Preliminary Results

5.1 Topology Optimization Results. Usually, a working TEG contains both P-type and N-type thermoelectric elements connected electrically in series and thermally in parallel. But single-type TEGs are also quite common and show great flexibility in practical applications. Thus, besides the P-type and N-type topology optimization formulation as described in Sec. 3, a single P-type optimization scenario is also considered. For one single P-type topology optimization, a mapped quadrilateral mesh with a maximum element size 0.3 mm is used. The total domain element number is 3468. The following topology optimization results in Figs. 5 and 6 are obtained by setting the volume fraction $V_f = 0.8$ and the external load $R = 0.1 \Omega$. The initial design is given such that $\rho_1 = V_f$ and $\rho_2 = 1$. With reference to Fig. 4(d), the results show that the relatively high-temperature thermoelectric materials Zn₄Sb₃ and CoSb₃ are distributed near the hot end, while the relatively lowtemperature thermoelectric materials Bi₂Te₃ near the cold end. In other words, each thermoelectric material is placed into its optimal working temperature interval to fully exploit their thermoelectric capability. Such materials distribution is not easy to obtain using the parametric studies as in, e.g., Refs. [16,50]. The maximum output power is 0.0589 W and 0.0198 W with the corresponding maximum conversion efficiency reaching 9.61% and 12.34% for these two scenarios, respectively. It is worth noticing that although more materials are employed, the conversion efficiency when both the P-type and N-type elements are optimized is quite smaller than that of single P-type element optimization.

The convergence curves for conversion efficiency and output power are displayed in Fig. 7 with the optimality tolerance set to be $5e^{-3}$. As expected, both objectives improve significantly compared with the initial designs. The clear boundary between different thermoelectric materials is achieved by setting up a threshold for ρ_1 and ρ_2 to distinguish one thermoelectric material from the other. However, one needs to be very careful applying this treatment,

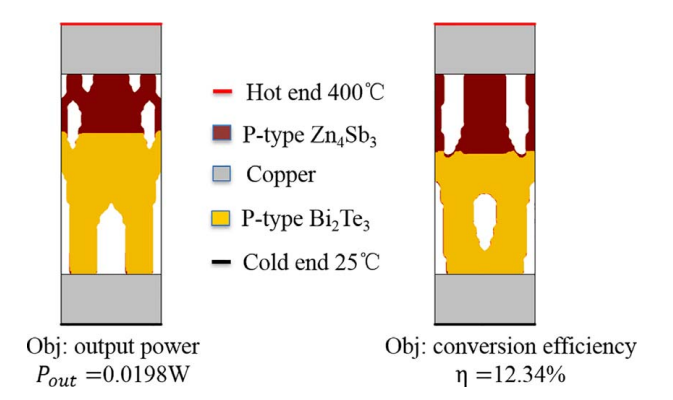


Fig. 6 Topology optimization with only P-type materials

0.9

0.8

0.7

0.6

0.5

0.4

0.3

0.2

0.1

0.9

0.8

0.7

0.6

0.5

0.4

0.3

0.2

0.1

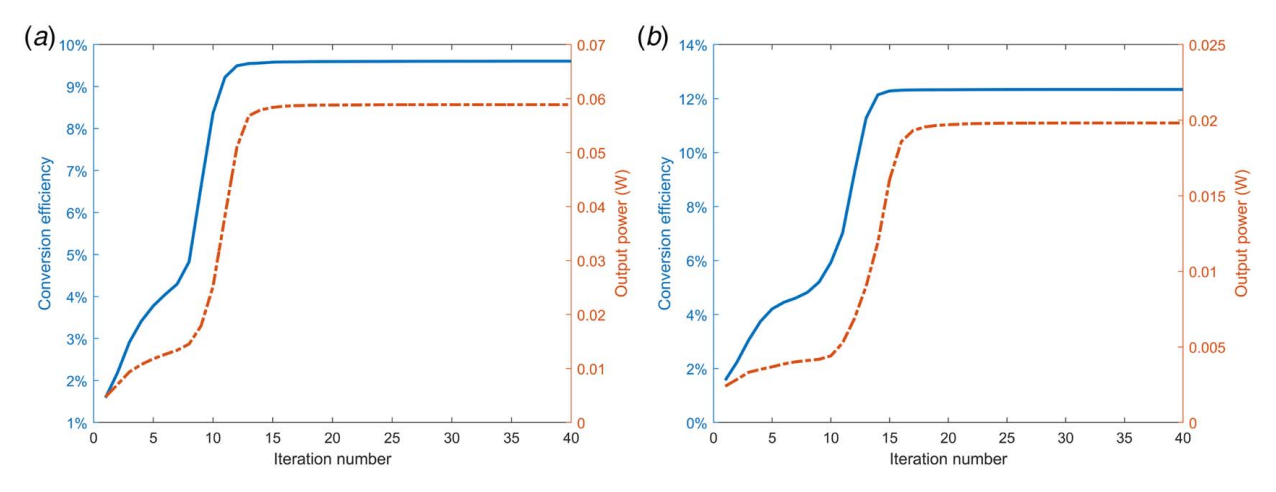


Fig. 7 Convergence history of the optimization process: (a) P-type and N-type optimization and (b) only P-type optimization

since there might exist gray regions representing the transition from one thermoelectric material to another. Such gray area are quite common in SIMP-based topology optimization methods and actually correspond to no physical materials. One approach of getting rid of these transition zones is the power-law as described in Sec. 3.3, in which a penalty factor is introduced in the interpolation scheme to penalize the intermediate density variables and force them to approach ρ_{\min} or 1.

As can be seen from Figs. 8 and 9, the actual distributions of the design variables ρ_1 and ρ_2 are given. Consulting the interpolation scheme in Sec. 3.3, the multiplication of $\rho_1^p \cdot \rho_2^p$ and $\rho_1^p \cdot (1 - \rho_2^p)$

correspond to different thermoelectric materials when their values equal to 1. Specifically, at a certain point, when $\rho_1^p \cdot (1-\rho_2^p)$ equals to 1, it is occupied by relatively high-temperature thermoelectric materials $\mathrm{Zn_4Sb_3}$ or $\mathrm{CoSb_3}$ depending on which type element it is. When $\rho_1^p \cdot \rho_2^p$ equals to 1, it is filled with $\mathrm{Bi_2Te_3}$. Even though the filter technique [51] is not adopted to mitigate the numerical instability like the so-called checkerboard problem, we can observe that the final designs are free of checkerboard pattern and there are only minor gray regions (circled area) in Figs. 8(a) and 8(b), where the aforementioned multiplications have the value between ρ_{\min} and 1. Such areas could have a negative

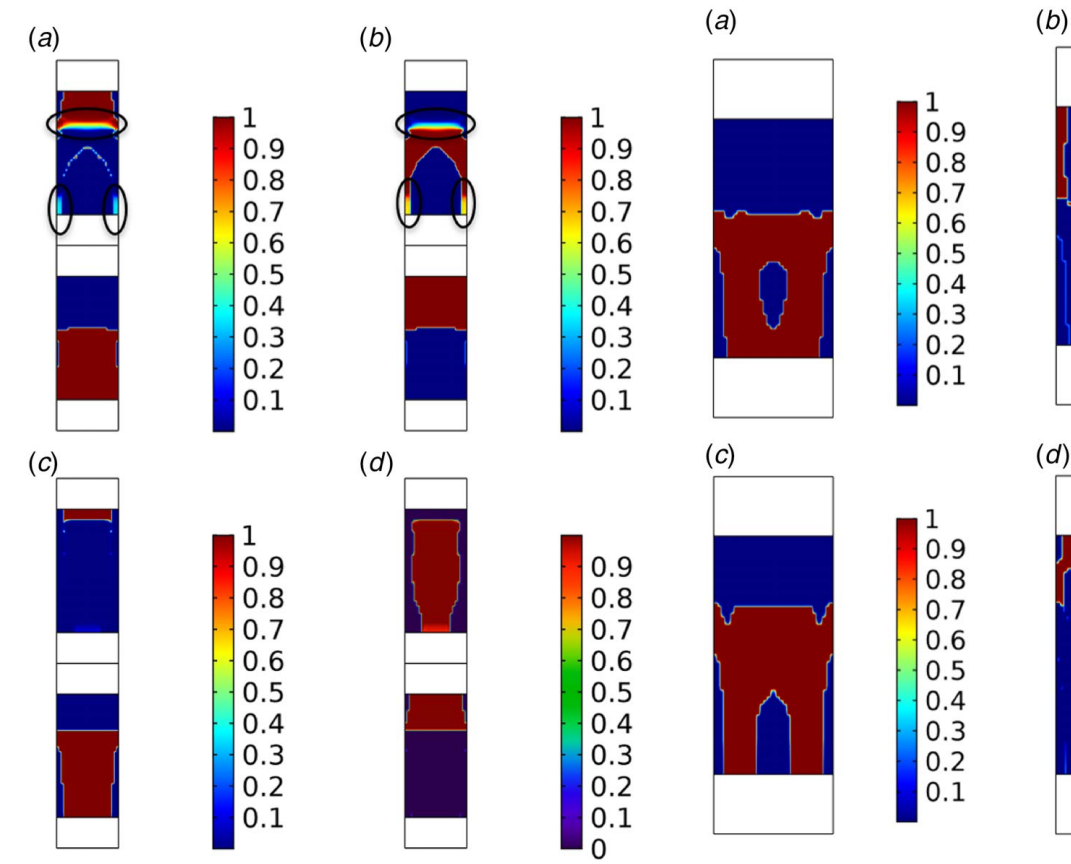


Fig. 8 The actual distribution of design variables of the P-type and N-type optimization: (a) plot of $\rho_1^p \cdot \rho_2^p$ with the conversion efficiency objective, (b) plot of $\rho_1^p \cdot (1-\rho_2^p)$ with the conversion efficiency objective, (c) plot of $\rho_1^p \cdot \rho_2^p$ with the output power objective, and (d) plot of $\rho_1^p \cdot (1-\rho_2^p)$ with the output power objective

Fig. 9 Actual distribution of design variables for only P-type optimization: (a) plot of ρ_1^p ρ_2^p when conversion efficiency is the objective function, (b) plot of ρ_1^p $(1-\rho_2^p)$ when conversion efficiency is the objective function, (c) plot of ρ_1^p ρ_2^p when output power is the objective function, and (d) plot of ρ_1^p $(1-\rho_2^p)$ when output power is the objective function

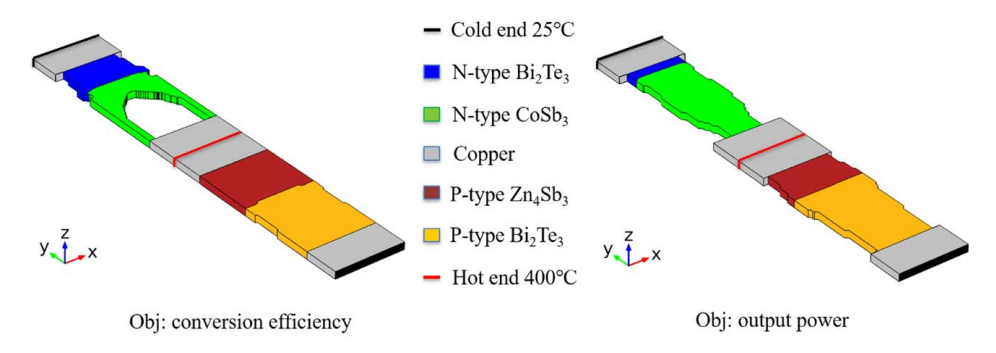


Fig. 10 2.5D model for P-type and N-type elements

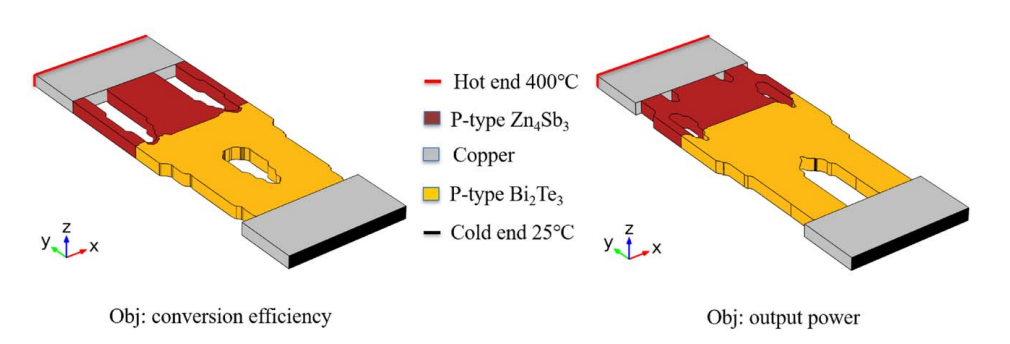


Fig. 11 2.5D model for only P-type element

influence on the actual performance of the optimized thermoelectric structures. Further, 2.5D verification is conducted in Sec. 5.2 to evaluate the effect. All remaining surfaces of $\rho_1^p \cdot \rho_2^p$ and $\rho_1^p \cdot (1-\rho_2^p)$ are free of gray regions, with the dark red area in the left and right part complementary to form what is present in Figs. 5 and 6. Such naturally clear boundary is strongly desired and we can expect good agreement between the topology optimization results and the 2.5D numerical verification, which will be covered in Sec. 5.2.

5.2 Numerical Verification. In this section, 2.5D models are built and simulated based on the optimized TEG structures obtained from the topology optimization algorithm proposed in this paper. As shown in Figs. 10 and 11, four models are established corresponding to the results for both output power and conversion efficiency as the objective functions with the volume fraction V_f =0.8. The overall dimensions are $60 \times 10 \times 1$ mm and $30 \times 10 \times 1$ mm for Figs. 10 and 11, respectively, which is consistent with the 2D geometry with a thickness of 1 mm as described in

Table 2 Performance verification of the optimization results

FEA verification (topology optimization)	Output power (W)	Conversion efficiency
P-type and N-type	0.0602 (0.0589)	9.58% (9.61%)
Only P-type	0.0209 (0.0198)	12.76% (12.34%)

Sec. 3.1. The same boundary conditions are applied as in Fig. 2. That is, for Fig. 10, the two end surfaces of copper are assigned low temperature with $T_c = 25$ °C, and the middle plane of the central copper electrode is treated as the hot end with $T_h = 400$ °C. While for Fig. 11, the boundary conditions for only P-type element apply. A zero electrical potential is placed on the lower end copper surface. And all other surfaces of the domain are prescribed as adiabatic and electrically insulated boundaries. The external resistor is still set to be $R = 0.1 \Omega$.

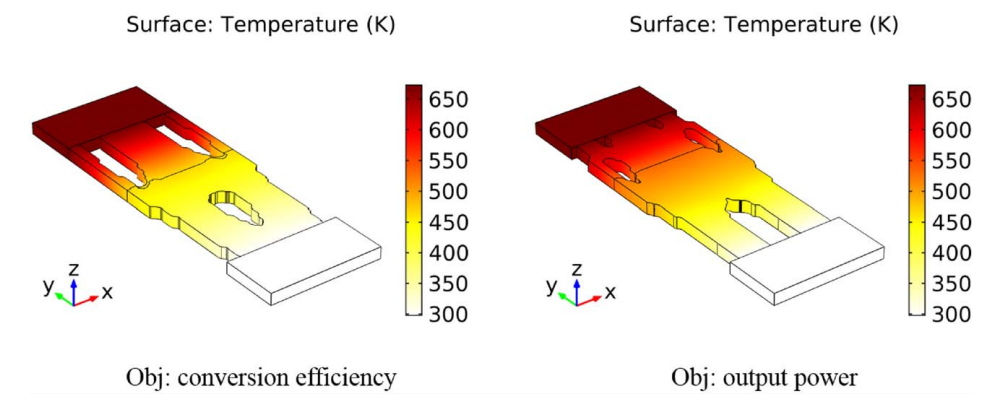


Fig. 12 Temperature distribution for only P-type structure

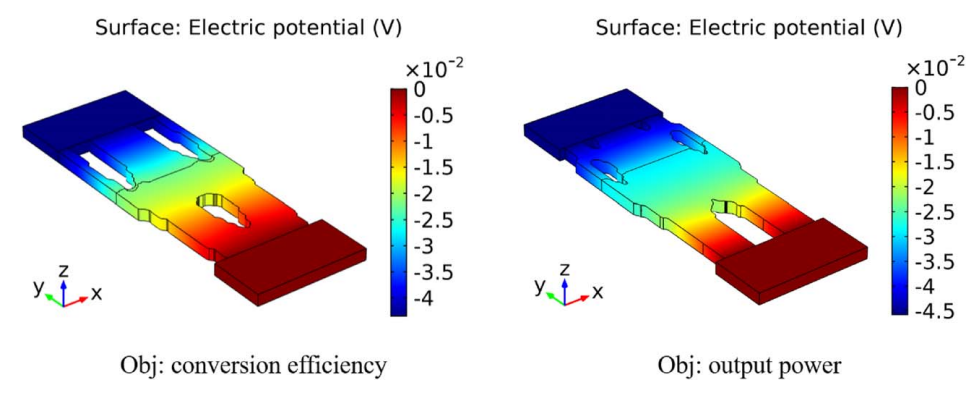


Fig. 13 Electrical potential distribution for only P-type structure

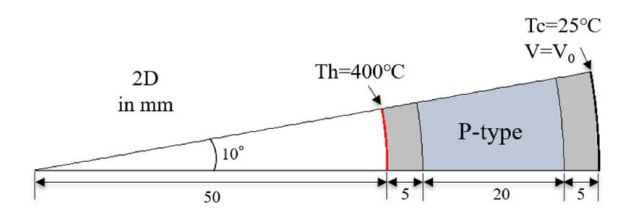


Fig. 14 Diagram for a fan-shaped TEG model

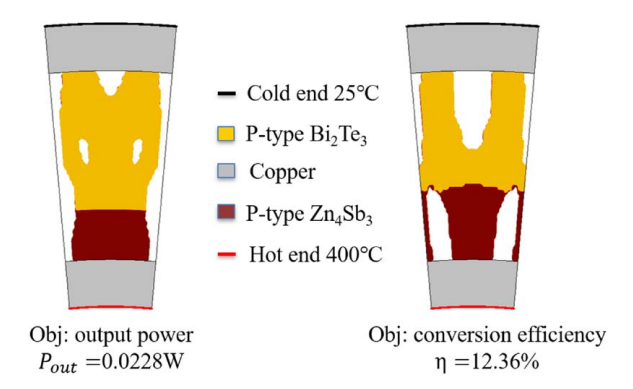


Fig. 15 Topology optimization results for fan-shaped TEG

From Table 2, the comparisons between the results obtained from topology optimization and 2.5D simulation show good agreement, which demonstrates the validity of the proposed methodology. And the effect of the above minor gray region on the actual performance of the optimized TEG structures is acceptable. For conciseness, the temperature and electrical potential distribution is only provided for P-type element optimization results as shown in Figs. 12 and 13.

6 A Conformal Thermoelectric Generator

The two topology optimization scenarios in Sec. 5 validated the proposed methodology with agreement between the 2.5D verification results and those obtained from topology optimization algorithm. Nevertheless, the design domains are relatively simple and regular. In practical applications, the geometry of the heat source (hot end) can be complicated, requiring the TEG unit conformal to that specific structure to achieve a better overall performance. Therefore, we further extend the proposed algorithm to design a TEG unit with a more irregular geometry as shown in Fig. 14. The fan-shaped TEG unit is intended for heat recovery for hot pipes, which usually have cylindrical shapes. Such TEG units can be attached to the hot pipes surface conformally to perfectly fit the heat source and facilitate the installation processes greatly as well as enhance the overall performance compared with the conventional planar TEG unit [52]. Similar to the computational model as described in Fig. 2, the temperature also ranges from 25 °C to 400 °C. The external load (not shown) is still fixed at $R = 0.1 \Omega$. The thickness is set to be 1 mm, and an electrical potential V_0 is assigned to the outer surface. The volume fraction V_f is still 0.8. For the fan-shaped TEG design, a mapped quadrilateral mesh with a maximum element size 0.3 mm is used. And the total domain element number is 4794.

The topology optimization results for the fan-shaped TEG are shown in Fig. 15. The maximum output power and conversion efficiency can reach 0.0228W and 12.36%, respectively. By extruding the results in the thickness direction for 1 mm, the 2.5D TEG unit is created as displayed in Fig. 16. In the 2.5D simulation, the two objective functions for the fan-shaped TEG are 0.0231 W and 12.70%, respectively, which are very close to those obtained from topology optimization. Then in Fig. 17, the recreated 2.5D fan-shaped TEG unit is mapped to a hot pipe surface conformally and connected electrically in series and thermally in parallel. The red cylindrical shell represents the hot pipe with the temperature 400 °C. The black outer surface is 25 °C representing the

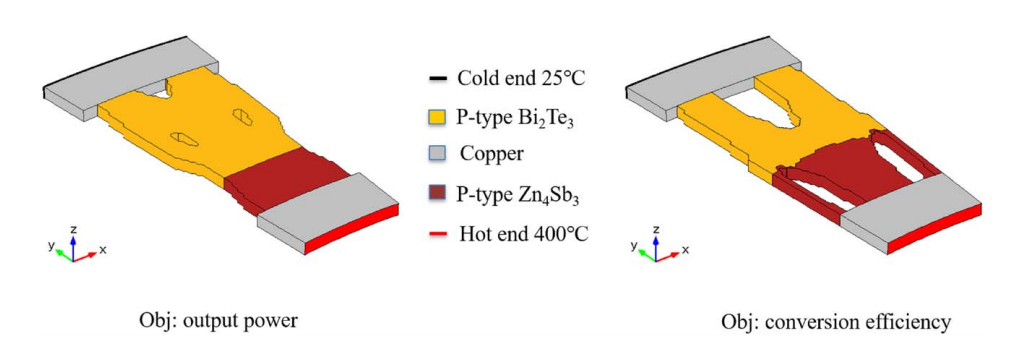


Fig. 16 2.5D models for fan-shaped TEG

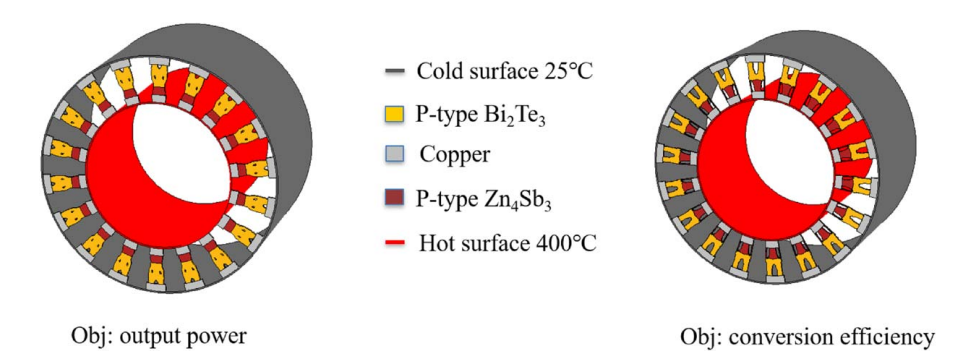


Fig. 17 A hot pipe embedded with optimized fan-shaped TEG units

atmosphere. For illustrative and conciseness purpose, there is only one layer of the fan-shaped TEG units in the axial direction. In practical scene, we can employ more TEG units to extend along the axial direction to produce more power. In the current architecture, there are in total 18 fan-shaped TEG units for each pipe. The external load is now changed to $R_1 = 18*R = 1.8 \Omega$. The simulated output power for the left pipe and conversion efficiency for the right pipe in Fig. 17 are 0.4102 W and 12.71% respectively. The output power is accumulation of 18 TEG units connected in series while the conversion efficiency remains nearly the same as a single TEG unit.

7 Conclusion and Future Work

In this paper, a SIMP-based topology optimization method is applied to the thermoelectric problems with the aim of maximizing the output power or conversion efficiency by optimizing the layouts of different thermoelectric materials in a prescribed domain. Bi₂Te₃ and Zn₄Sb₃ are selected for P-type element while Bi₂Te₃ and CoSb₃ for N-type element. The temperature varies from 25 °C at cold end to 400 °C at hot end. Two optimization scenarios with relatively regular domains are first considered with one case optimizing on both P-type and N-type elements simultaneously, and the other one only on single P-type element. The optimized output power is 0.0589 W and 0.0198 W with the corresponding maximum conversion efficiency reaching 9.61% and 12.34% for these two scenarios, respectively, which is quite promising when compared with the results from Ref. [14]. 2.5D simulation results match those obtained from topology optimization quite well with only acceptable discrepancies, which demonstrates the validity of the proposed methodology.

Then, we extend the proposed topology optimization algorithm to more irregular TEG design domains. A fan-shaped TEG unit containing only P-type element is optimized. The optimized output power and conversion efficiency could reach 0.0228W and 12.36%, respectively. Afterward, the optimized fan-shaped TEG units are conformally mapped to a cylindrical hot pipe surface to harvest the waste heat, and the simulated output power and conversion efficiency are in consistence with those from single TEG unit simulation.

However, there are still several aspects that can be improved. Practical experiments should be carried out to further verify the proposed method. Second, although the fan-shaped TEG is in relatively irregular geometry, it is still developable. In practical applications, the design domains can be undevelopable, e.g., free-form surfaces, requiring the optimized TEG conformal to that specific structure. In that sense, we need to resolve the topology optimization problems of TEGs on free-form surfaces, which usually is not an easy task. Conformal mapping theory has recently been integrated into the field of topology optimization [53,54]. It shows a lot of potential in solving such topology optimization problems on manifolds.

Acknowledgment

The authors acknowledge the support from the National Science Foundation (Grant Nos. CMMI1462270, CMMI1762287, and ECCS1508862), Ford University Research Program (URP) (Award No. 2017-9198R), and the start-up grant from the State University of New York at Stony Brook.

References

- Snyder, G. J., and Toberer, E. S., 2008, "Complex Thermoelectric Materials," Nat. Mater., 7(2), p. 105.
- [2] Zhang, X., and Zhao, L.-D., 2015, "Thermoelectric Materials: Energy Conversion Between Heat and Electricity," J. Materiom., 1(2), pp. 92–105.
- [3] O'Brien, R., Ambrosi, R., Bannister, N., Howe, S., and Atkinson, H. V., 2008, "Safe Radioisotope Thermoelectric Generators and Heat Sources for Space Applications," J. Nucl. Mater., 377(3), pp. 506–521.
- [4] Kumar, S., Heister, S. D., Xu, X., Salvador, J. R., and Meisner, G. P., 2013, "Thermoelectric Generators for Automotive Waste Heat Recovery Systems Part I: Numerical Modeling and Baseline Model Analysis," J. Electron. Mater., 42(4), pp. 665–674.
- [5] Kumar, S., Heister, S. D., Xu, X., Salvador, J. R., and Meisner, G. P., 2013, "Thermoelectric Generators for Automotive Waste Heat Recovery Systems Part II: Parametric Evaluation and Topological Studies," J. Electron. Mater., 42(6), pp. 944–955.
- [6] Champier, D., 2017, "Thermoelectric Generators: A Review of Applications," Energy Convers. Manage., 140, pp. 167–181.
- [7] He, W., Zhang, G., Zhang, X., Ji, J., Li, G., and Zhao, X., 2015, "Recent Development and Application of Thermoelectric Generator and Cooler," Appl. Energy, 143, pp. 1–25.
- [8] Bell, L. E., 2008, "Cooling, Heating, Generating Power, and Recovering Waste Heat With Thermoelectric Systems," Science, 321(5895), pp. 1457–1461.
- [9] Zhao, L.-D., Lo, S.-H., Zhang, Y., Sun, H., Tan, G., Uher, C., Wolverton, C., Dravid, V. P., and Kanatzidis, M. G., 2014, "Ultralow Thermal Conductivity and High Thermoelectric Figure of Merit in SnSe Crystals," Nature, 508(7496), p. 373.
- [10] Biswas, K., He, J., Blum, I. D., Wu, C.-I., Hogan, T. P., Seidman, D. N., Dravid, V. P., and Kanatzidis, M. G., 2012, "High-Performance Bulk Thermoelectrics With All-Scale Hierarchical Architectures," Nature, 489(7416), p. 414.
- [11] Hicks, L., and Dresselhaus, M. S., 1993, "Effect of Quantum-Well Structures on the Thermoelectric Figure of Merit," Phys. Rev. B, 47(19), p. 12727.
- [12] Pei, Y., Wang, H., and Snyder, G. J., 2012, "Band Engineering of Thermoelectric Materials," Adv. Mater., 24(46), pp. 6125–6135.
- [13] He, J., Kanatzidis, M. G., and Dravid, V. P., 2013, "High Performance Bulk Thermoelectrics Via a Panoscopic Approach," Mater. Today, 16(5), pp. 166–176.
- [14] El-Genk, M. S., and Saber, H. H., 2003, "High Efficiency Segmented Thermoelectric Unicouple for Operation Between 973 and 300 K," Energy Convers. Manage., 44(7), pp. 1069–1088.
- [15] Snyder, G. J., 2004, "Application of the Compatibility Factor to the Design of Segmented and Cascaded Thermoelectric Generators," Appl. Phys. Lett., 84(13), pp. 2436–2438.
- [16] Hadjistassou, C., Kyriakides, E., and Georgiou, J., 2013, "Designing High Efficiency Segmented Thermoelectric Generators," Energy Convers. Manage., 66, pp. 165–172.
- [17] Snyder, G. J., and Ursell, T. S., 2003, "Thermoelectric Efficiency and Compatibility," Phys. Rev. Lett., 91(14), p. 148301.
 [18] Takezawa, A., and Kitamura, M., 2012, "Geometrical Design of Thermoelectric
- [18] Takezawa, A., and Kitamura, M., 2012, "Geometrical Design of Thermoelectric Generators Based on Topology Optimization," Int. J. Numer. Methods Eng., 90(11), pp. 1363–1392.
- [19] Soprani, S., Haertel, J. H. K., Lazarov, B. S., Sigmund, O., and Engelbrecht, K., 2016, "A Design Approach for Integrating Thermoelectric Devices using Topology Optimization," Appl. Energy, 176, pp. 49–64.

- [20] Mativo, J., and Hallinan, K., 2019, "Development of Compliant Thermoelectric Generators (tegs) in Aerospace Applications using Topology Optimization,' Energy Harvesting Syst., 4(2), pp. 87-105.
- [21] Lundgaard, C., and Sigmund, O., 2018, "A Density-Based Topology Optimization Methodology for Thermoelectric Energy Conversion Problems, Struct. Multidiscip. Optim., 57(4), pp. 1427–1442.
- [22] Lundgaard, C., Sigmund, O., and Bjørk, R., 2018, "Topology Optimization of Segmented Thermoelectric Generators," J. Electronic Mater., 47(12), pp. 6959-
- [23] Lundgaard, C., and Sigmund, O., 2019, "Design of Segmented Off-Diagonal Thermoelectric Generators using Topology Optimization," Appl. Energy, 236, pp. 950–960.
- [24] Lundgaard, C., and Sigmund, O., 2019, "Design of Segmented Thermoelectric
- Peltier Coolers by Topology Optimization," Appl. Energy, 239, pp. 1003–1013. [25] Bendsøe, M. P., and Kikuchi, N., 1988, "Generating Optimal Topologies in Structural Design Using a Homogenization Method," Comput. Methods Appl. Mech. Eng., **71**(2), pp. 197–224.
- [26] Bendsøe, M. P., 1989, "Optimal Shape Design As a Material Distribution Problem," Struct. Optim., 1(4), pp. 193–202.
- [27] Zhou, M., and Rozvany, G., 1991, "The COC Algorithm, Part II: Topological, Geometrical and Generalized Shape Optimization," Comput. Methods Appl. Mech. Eng., 89(1-3), pp. 309-336.
- [28] Allaire, G., Jouve, F., and Toader, A.-M., 2004, "Structural Optimization Using Sensitivity Analysis and a Level-set Method," J. Comput. Phys., 194(1), pp. 363-393.
- [29] Wang, M. Y., Wang, X., and Guo, D., 2003, "A Level Set Method for Structural Topology Optimization," Comput. Methods Appl. Mech. Eng., 192(1-2), pp. 227-246.
- [30] Norato, J., Bell, B., and Tortorelli, D. A., 2015, "A Geometry Projection Method for Continuum-Based Topology Optimization with Discrete Elements," Comput. Methods Appl. Mech. Eng., 293, pp. 306-327.
- [31] Norato, J., Haber, R., Tortorelli, D., and Bendsøe, M. P., 2004, "A Geometry Projection Method for Shape Optimization," Int. J. Numer. Methods Eng., 60(14), pp. 2289-2312.
- [32] Zhang, S., Norato, J. A., Gain, A. L., and Lyu, N., 2016, "A Geometry Projection Method for the Topology Optimization of Plate Structures," Struct. Multidiscip. Optim., 54(5), pp. 1173-1190.
- [33] Kazemi, H., Vaziri, A., and Norato, J. A., 2018, "Topology Optimization of Structures Made of Discrete Geometric Components with Different Materials," ASME J. Mech. Des., 140(11), p. 111401.
- [34] Guest, J. K., 2009, "Topology Optimization with Multiple Phase Projection,"
- Comp. Methods Appl. Mech. Eng., 199(1-4), pp. 123–135. [35] Guo, X., Zhang, W., and Zhong, W., 2014, "Doing Topology Optimization Explicitly and Geometrically-A New Moving Morphable Components Based Framework," ASME J. Appl. Mech., 81(8), p. 081009.
- [36] Zhang, W., Yuan, J., Zhang, J., and Guo, X., 2016, "A New Topology Optimization Approach Based on Moving Morphable Components (MMC) and the Ersatz Material Model," Struct. Multidiscip. Optim., 53(6), pp. 1243-1260.

- [37] Zhang, W., Song, J., Zhou, J., Du, Z., Zhu, Y., Sun, Z., and Guo, X., 2018, "Topology Optimization with Multiple Materials Via Moving Morphable Component (MMC) Method," Int. J. Numer. Methods Eng., 113(11), pp. 1653-
- [38] Bourdin, B., and Chambolle, A., 2003, "Design-Dependent Loads in Topology Optimization," ESAIM: Control Optim. Calculus Var., 9, pp. 19-48.
- [39] Xie, Y. M., and Steven, G. P., 1993, "A Simple Evolutionary Procedure for Structural Optimization," Comput. Struct., 49(5), pp. 885–896.
- [40] Dede, E. M., Joshi, S. N., and Zhou, F., 2015, "Topology Optimization, Additive Layer Manufacturing, and Experimental Testing of An Air-Cooled Heat Sink," ASME J. Mech. Des., 137(11), p. 111403.
- [41] Fuchi, K., and Diaz, A. R., 2013, "Origami Design by Topology Optimization," ASME J. Mech. Des., 135(11), p. 111003.
- [42] Fu, J., Xia, L., Gao, L., Xiao, M., and Li, H., 2019, "Topology Optimization of Periodic Structures with Substructuring," ASME J. Mech. Des., 141(7), p. 071403.
- [43] Svanberg, K., 1987, "The Method of Moving Asymptotes—A New Method for
- Structural Optimization," Int. J. Numer. Methods Eng., 24(2), pp. 359–373. [44] Landau, L. D., Bell, J., Kearsley, M., Pitaevskii, L., Lifshitz, E., and Sykes, J., 2013, Electrodynamics of Continuous Media, Vol. 8, Elsevier, Amsterdam.
- [45] Bendsøe, M. P., and Sigmund, O., 2013, Topology Optimization: Theory, Methods, and Applications, Springer Science and Business Media, Berlin.
- [46] Zuo, W., and Saitou, K., 2017, "Multi-Material Topology Optimization Using
- Ordered SIMP Interpolation," Struct. Multidiscip. Optim., 55(2), pp. 477-491. Kajikawa, T., Rowe, D., and Rowe, D., 2006, Thermoelectric Handbook: Macro
- to Nano, CRC/Taylor & Francis, Boca Raton, FL, USA [48] Zienkiewicz, O. C., Taylor, R. L., Zienkiewicz, O. C., and Taylor, R. L., 1977, The Finite Element Method, Vol. 36, McGraw-Hill, London.
- Allaire, G., 2015, "A Review of Adjoint Methods for Sensitivity Analysis, Uncertainty Quantification and Optimization in Numerical Codes," Ingénieurs de l'Automobile, 836, pp. 33-36.
- [50] Wu, Y., Yang, J., Chen, S., and Zuo, L., 2018, "Thermo-Element Geometry Optimization for High Thermoelectric Efficiency," Energy, 147, pp. 672–680.
- [51] Bourdin, B., 2001, "Filters in Topology Optimization," Int. J. Numer. Methods Eng., 50(9), pp. 2143-2158
- [52] Kim, F., Kwon, B., Eom, Y., Lee, J. E., Park, S., Jo, S., Park, S. H., Kim, B.-S., Im, H. J., Lee, M. H., Min, T. K., Kim, K. T., Chae, H. G., king, W. P., and Son, J. S., 2018, "3D Printing of Shape-Conformable Thermoelectric Materials Using All-Inorganic Bi 2 Te 3-Based Inks," Nat. Energy, 3(4), pp. 301-309.
- [53] Ye, O., Guo, Y., Chen, S., Lei, N., and Gu, X. D., 2019, "Topology Optimization of Conformal Structures on Manifolds Using Extended Level Set Methods (X-LSM) and Conformal Geometry Theory," Comput. Methods Appl. Mech. Eng., 344, pp. 164-185.
- [54] Jiang, L., Guo, Y., Chen, S., Wei, P., Lei, N., and Gu, X. D., 2019, "Concurrent Optimization of Structural Topology and Infill Properties With a CBF-Based Level Set Method," Front. Mech. Eng. China, 14(2), pp. 171-189.